OPEN ACCESS

ARTICLE

Journal homepage: www.the-innovation.org/energy-use

Energy Use

INNOVATION PRESS

Energy Use 1 (2025):100005

Contents lists available at INNOVATION PRESS

A Model-Based EV Driving Range Assessment with Genetic-Algorithm-Optimized Motor Waste Heat Recovery Strategies

Lige Zhao,[1] **Parastoo Mohebi,**[1] **and Zhe Wang**[1,*]

*Correspondence: cezhewang@ust.hk

Received: August 22, 2025; Accepted: September 12, 2025; Published Online: September 25, 2025; https://doi.org/10.59717/ipj.energy-use.2025.100005

GRAPHICAL ABSTRACT

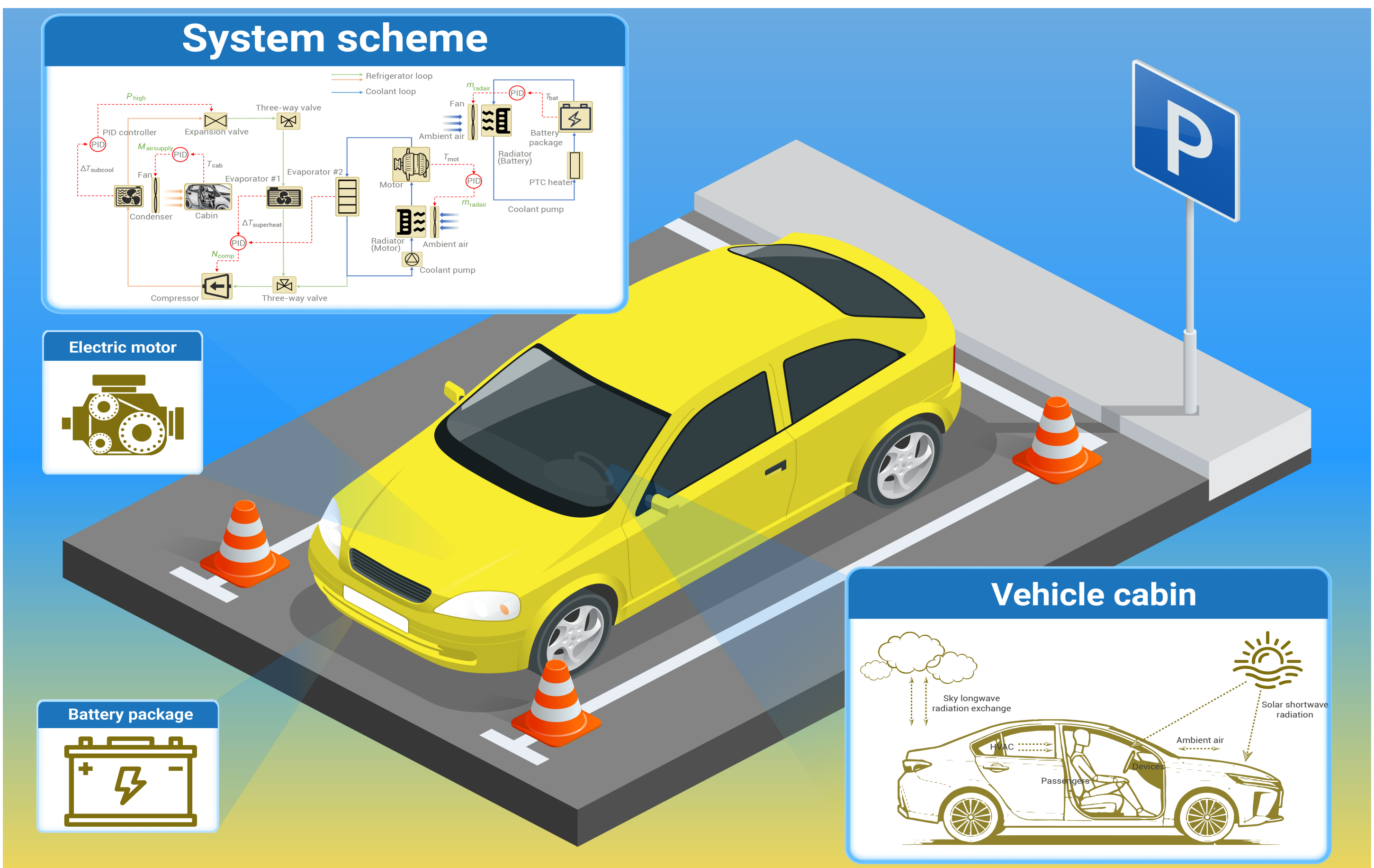

PUBLIC SUMMARY

- A plug-and-play vehicle-thermal co-simulation platform assesses TMS impacts.
- TMS (Thermal Management System) cuts EV range 12–16% in summer, 25–31% in winter.
- Cabin shell heat load dominates year-round; >80% in winter drives heat pump use.
- Range varies near-linearly with ambient, occupants, absorptivity, transmittivity.
- WHR (Waste Heat Recovery) saves more in steady state; S1 outperforms S2; GA guides tuning.

ARTICLE

Journal homepage: www.the-innovation.org/energy-use

Energy Use

INNOVATION PRESS

Energy Use 1 (2025):100005

Contents lists available at INNOVATION PRESS

A Model-Based EV Driving Range Assessment with Genetic-Algorithm-Optimized Motor Waste Heat Recovery Strategies

Lige Zhao,[1] Parastoo Mohebi,[1] and Zhe Wang[1,*]

[1]Department of Civil and Environmental Engineering, The Hong Kong University of Science and Technology, Hong Kong SAR, China

*Correspondence: cezhewang@ust.hk

Received: August 22, 2025; Accepted: September 12, 2025; Published Online: September 25, 2025; https://doi.org/10.59717/ipj.energy-use.2025.100005

Citation: Zhao L., Mohebi P. and Wang Z. (2025). A Model-Based EV Driving Range Assessment with Genetic-Algorithm-Optimized Motor Waste Heat Recovery Strategies. *Energy Use* **1**:100005.

This study develops a coupled vehicle-thermal management simulation platform integrating FASTSim dynamics, reduced-order thermal models, and an R134a air-source heat pump (ASHP) to evaluate the impact of thermal management system (TMS) on EV energy consumption and optimize motor waste heat recovery (WHR) in winter. Simulation results under the WLTP cycle show that TMS activation reduces driving range by 12% to 16% in summer and 25% to 31% in winter, with cabin envelope heat load being the dominant factor ($>$80% in winter) and ambient temperature the most influential external parameter. Three heating modes are compared: S0 (pure ASHP), S1 (on-off WHR controlled by T_{on}/T_{off}), and S2 (dual-source WHR regulated by Q_{whr}). Using genetic algorithm (GA) to minimize average TMS power under hard constraints, optimal S1 and S2 strategies at −5°C reduce heat pump energy consumption (excluding battery PTC) by 16% and 9% respectively versus S0, corresponding to range gains of 1.8% and 1.0%. Immediate heat recovery after cold start is suboptimal; S1 requires delayed activation with sufficient hysteresis, while S2 exhibits a clear Q_{whr} trade-off. Overall winter energy savings are constrained by dominant battery PTC consumption during warm-up, becoming more significant during steady-state operation. These findings provide quantitative insights for WHR parameter tuning and strategy mapping based on operational conditions.

INTRODUCRTION

Research background

The promotion and widespread adoption of electric vehicles (EVs) play a crucial role in achieving carbon neutrality goals.[1] Compared to traditional internal combustion engine vehicles, EVs can significantly reduce greenhouse gas emissions and air pollutants,[2] aiding nations worldwide in meeting their environmental sustainability targets. However, the limited capacity of batteries constrains the driving range of EVs.[3] For EV manufacturers, extending the driving range poses a challenging issue.[4] Accurately predicting the remaining range during driving is important for helping drivers plan their trips, making it a vital topic in the EV industry.[5,6] The thermal management system (TMS) is a major energy-consuming unit,[7] accounting for 20% of total energy consumption under typical driving conditions and up to 60% in traffic jams or cold weather.[8] The TMS in EVs is responsible for the cooling and heating of the vehicle cabin, battery pack, and electric motor, impacting not only vehicle efficiency but also the operational safety of key components.[9] For the cabin, the TMS aims to provide a comfortable thermal environment for the driver and passengers,[10] significantly influencing driver behavior and fatigue levels.[11] Based on the configuration and operation of its components, the TMS can be categorized into separate systems and integrated systems.[12] And for the system solutions, the vapor compression heat pump has become a widely adopted air conditioning technology in EVs in recent years.[13] This solution, utilizing a four-way valve to switch between cooling and heating, offers compactness and generally higher heating efficiency than PTC (Positive Temperature Coefficient) heating.[14]

Modeling is a highly efficient research method for studying EV TMS. For manufacturers, modeling can aid in the system-level optimization of the TMS during the vehicle design phase.[15] For researchers, using models instead of actual vehicles can save substantial resources.[16] A vehicle-level TMS model integrates models of the cabin, battery, motor, and heat pump system. Coupling these models with the vehicle's powertrain allows for a comprehensive evaluation of the TMS's performance under driving conditions.[17] Among these subsystems, the cabin thermal environment model is the most complex. The cabin's thermal load is influenced by external conditions, the thermal properties of the vehicle body, driving speed, occupant number, and comfort requirements.[18] Methods for modeling the cabin thermal environment include physical models and data-driven models. Physical models comprise high-fidelity 3-D CFD models and computationally efficient lumped parameter models,[19,20] while data-driven models can achieve excellent simulation accuracy with sufficient training data,[21] relying less on expert knowledge. In the study of vehicle-level TMS and its impact on driving range, lumped parameter models, with their superior computational speed and relatively simple structure, are the primary method for cabin thermal environment simulation, as detailed 3D spatial temperature distribution simulations are often unnecessary for system energy consumption analysis.[22]

Existing work and research objectives

Currently, there is extensive research on model-based integrated thermal management systems (iTMS) for EVs, especially for the driving mileage assessment. Horrein et al. developed a multi-domain EV model to analyze the interactions between the powertrain and the TMS, finding that driving range decreases by nearly 30% under winter heating conditions.[23] Penning et al. studied the impact of window glass parameters on the TMS and overall vehicle performance using an integrated EV model and found that vehicles equipped with high-performance glass had a driving range approximately 33 miles longer than those with ordinary glass under strong solar radiation.[24] Xu et al. combined an EV TMS model with the FASTSim tool developed by the National Renewable Energy Laboratory (NREL) to conduct a parametric study of driving range under cooling conditions in summer.[25,26] The results showed that the TMS could reduce the driving range by 38-45% in UDDS cycle. Unlike conventional internal combustion engine vehicles that utilize waste heat from engine combustion for cabin heating in winter, EVs typically rely on PTC heaters and air-source heat pump systems (ASHP). This inevitably increases the vehicle's energy burden and exacerbates range anxiety during cold weather. To mitigate heating energy consumption, researchers have proposed recovering waste heat from the electric motor and other control

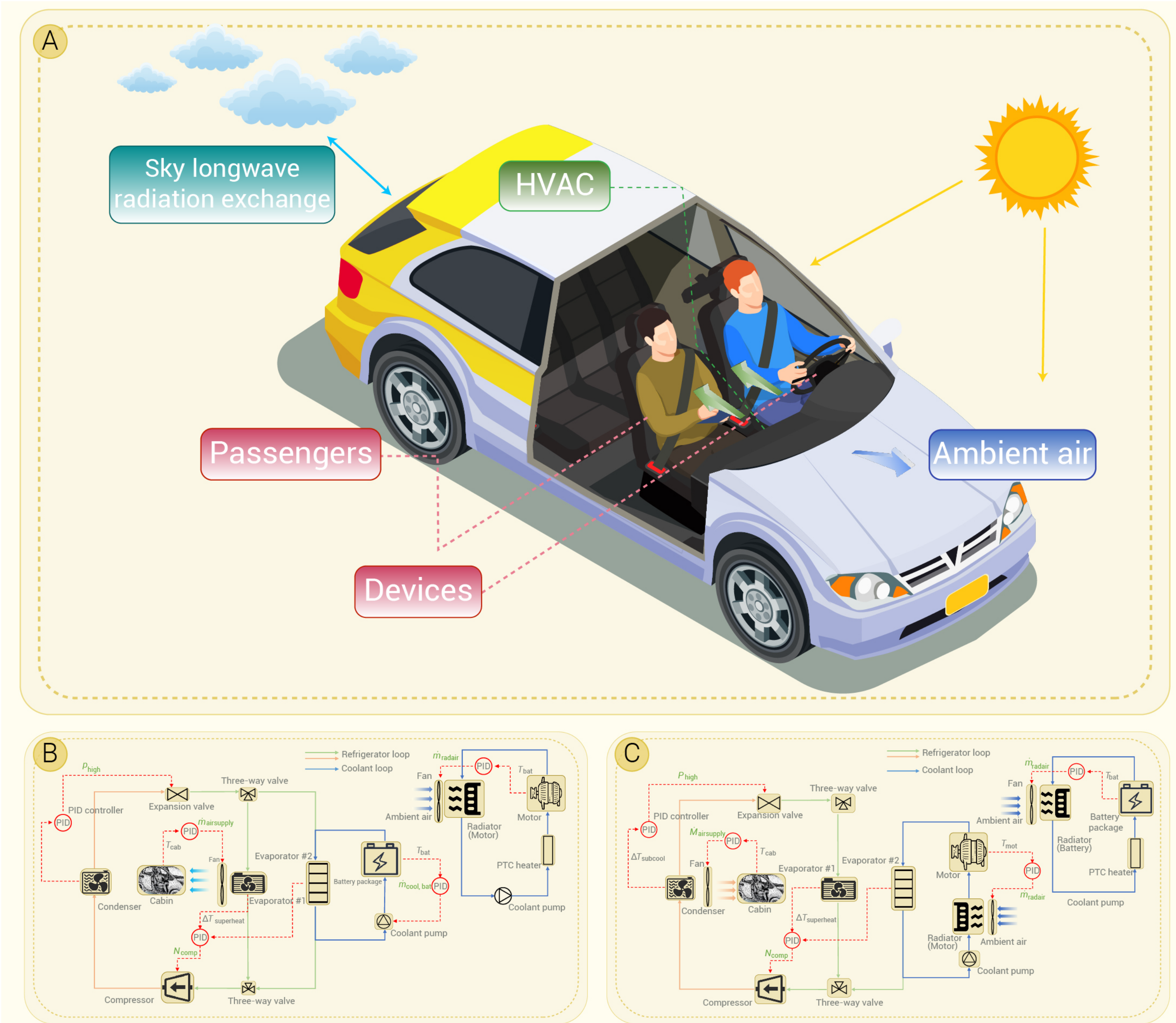

Figure 1. Overview of cabin thermal model. (A) Vehicle cabin thermal model. (B) TMS scheme: summer. (C) TMS scheme: winter.

units.[27] Model-based calculations indicate that such waste heat recovery (WHR) can improve the system coefficient of performance (COP) by 13.2%. Building upon the theoretical foundation of WHR, further strategies involving multi-source and segmented WHR systems for EVs have been investigated. Lee et al. evaluated the performance of a heat recovery system under different temperature levels and employed model predictive control to recover heat at optimal temperatures, achieving a 13% reduction in EV power consumption compared to conventional WHR systems.[28] Liu et al. proposed a segmented heating strategy utilizing three heat sources: motor waste heat, ambient air, and a PTC heater. This strategy reduced energy consumption by 18.49% during a 2.5-hour operation at an ambient temperature of −10 °C.[29] Qiao et al. developed a segmented heating strategy based on battery temperature, utilizing heat sources including the PTC heater, ambient air, battery, and motor waste heat. After 2.2 hours of operation at −7 °C, energy consumption reductions of 6.2% and 3.7% were achieved under different conditions.[30]

However, existing research on motor WHR predominantly relies on rule-based or expert-experience strategies. There is insufficient discussion on their adaptability and transferability across diverse environmental conditions and driving cycles, and no definitive optimal WHR operating strategy has been established. Therefore, this paper focuses on an ASHP-based EV HVAC system integrated with a motor WHR solution on the evaporator side. We formulate the winter WHR scheduling problem as a parametric strategy optimization problem. A Genetic Algorithm (GA) is employed for offline optimization within a modeled co-simulation framework. GA is a derivative-free, population-based global optimization method capable of robust performance on non-convex, non-differentiable, black-box objectives (evaluated solely via coupled simulation).[31] Its inherent suitability for parallel computation makes it well-suited for rapidly approximating optimal solutions within low-dimensional strategy parameter spaces. The main contributions of this study are as follows:

1) Modular Vehicle-Thermal Management Co-Simulation Framework: Constructs and couples the powertrain, a reduced-order cabin thermal model, battery/motor thermal models, and a vapor-compression heat pump system with WHR, forming a reusable co-simulation platform for rapid evaluation across different vehicles, TMS topologies, environments, and driving cycles.

2) Quantitative System Assessment and Sensitivity Analysis for Range Evaluation: Evaluates the seasonal impact of the TMS on driving range under unified models and operating conditions. Provides sensitivity results for key

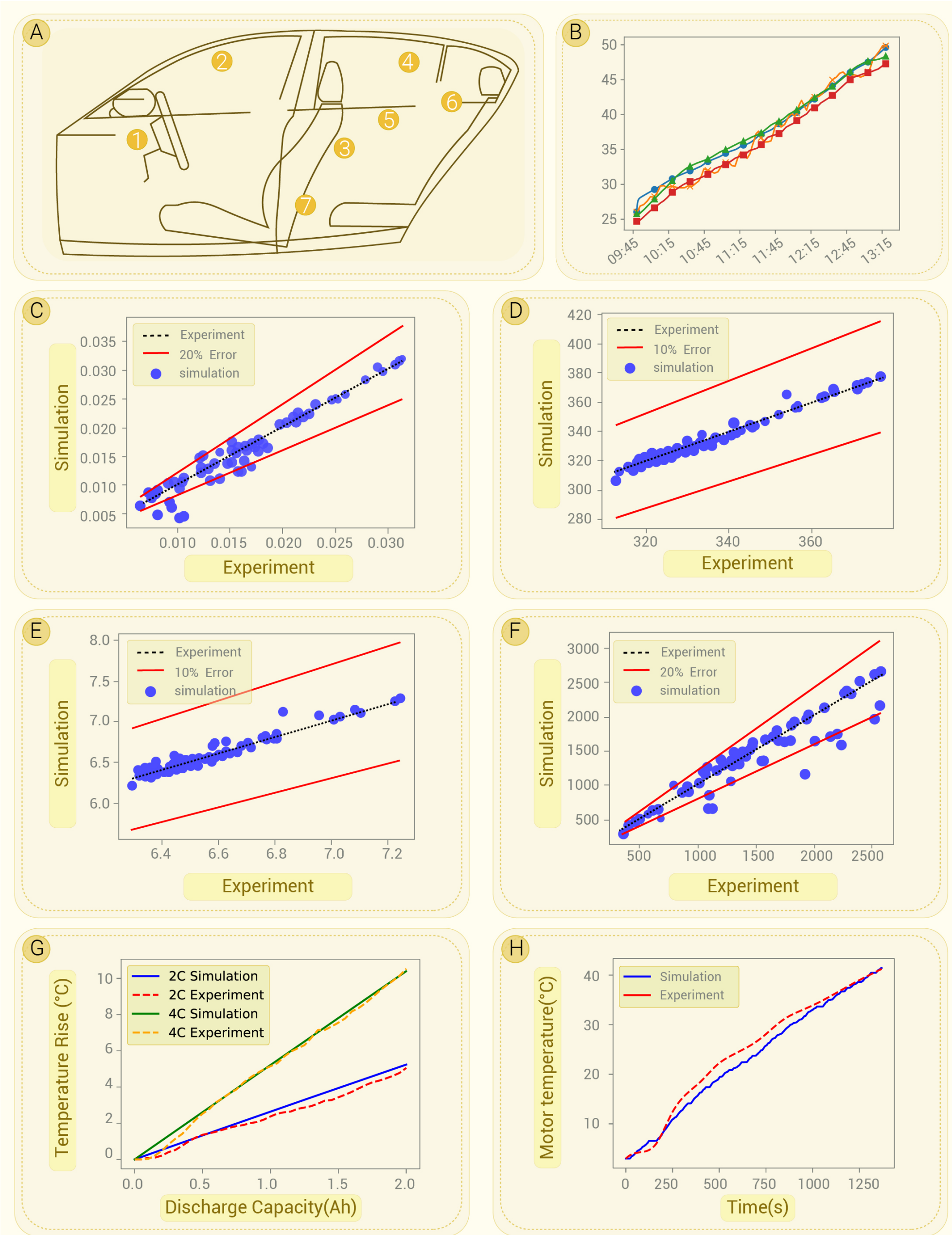

Figure 2. Cabin model validation. (A) Sensor location. (B) Results comparison. (C) Refrigerant mass flow rate (kg/s). (D) Condensing temperature (K). (E) Refrigerant enthalpy after compressor (×105 J/kg). (F) Compressor power (W).

external disturbances, establishing a baseline context for understanding and comparing WHR optimization benefits.

3) Physics-Informed Parameterization of WHR Strategy: Explicitly identifies the core trade-offs between energy efficiency, recoverable heat quantity, and recovery duration, governed by evaporation temperature/pressure ratio, PTC substitution level, and motor thermal capacitance.

4) GA-Optimized Offline Strategy and Baseline Validation: Solves for optimal WHR parameters under representative winter environments and driving cycles using GA. Validates results by comparing baseline heating strategies, quantifying improvements in TMS energy consumption and driving range.

5) Mapping from Offline Optima to Deployable Strategies: Derives a concise mapping from operating condition features to optimal strategy parameters based on multi-scenario offline optimization results. This provides practical engineering tuning guidelines without requiring online optimization.

Model description

The models adopted in this study include a powertrain model and an iTMS model. The function of the powertrain model is to simulate the vehicle's driving performance based on the drag coefficient, propulsion system parameters, road conditions, and driving cycle conditions. In the powertrain model, the propulsion system also provides real-time feedback on energy consumption and charging status to the battery pack. The powertrain model is based on the Python version of the FASTSim tool developed by NREL,[26] and the vehicle powertrain parameters refer to Tesla Model 3. The iTMS model comprises a detailed cabin thermal environment model, a battery pack and motor thermal dynamics model, and ASHP model with motor WHR. The vehicle geometry parameters are obtained from the Tesla official website, while the thermal-physical properties of all the vehicle components and heat transfer coefficients are sourced from other studies stated in Table S1.

Thermal load

Vehicle cabin. The cabin thermal environment model is the most critical component of the TMS model because the cabin thermal load is the largest energy consumption source for the HVAC system. As shown in Figure 1A, throughout all seasons of the year, an outdoor parked or driving EV's cabin thermal environment involves multiple sources of thermal load. The temperature inside the cabin is influenced by various internal and external environmental factors.[32] External loads include thermal loads from radiation and convection, while internal loads include heat dissipation from the driver and passengers and heat from electronic devices inside the vehicle. In the cabin model of this study, the temperature change of the air inside the cabin, the cabin shell, and the internal mass such as the seats are all considered to ensure the model accuracy. The effect of sky long wave radiation contributes little to the thermal load, so this term is ignored in this study. The temperature changes are influenced not only by internal and external thermal loads but also by heat exchange among these three components. The key parameters are indicated in Table S1.[25,32,35]

Cabin shell: For the cabin shell, thermal load includes solar radiation heat gain on its surfaces $Q_{sol,sh}$, convective heat transfer with the ambient air Q_{e-sh}, radiative heat transfer with the internal mass Q_{m-sh}, convective heat transfer between the shell and the cabin air Q_{a-sh}. These factors influence the overall temperature changes of the cabin shell. The governing equations of cabin shell model are as follows:

$$m_{sh}c_{sh}\frac{dT_{sh}}{dt} = Q_{sol,sh} + Q_{e-sh} + Q_{m-sh} + Q_{a-sh} \tag{1}$$

$$Q_{sol,sh} = \alpha_{sh}(I_{dir} + I_{dif})A_{rad,sh} \tag{2}$$

$$Q_{e-sh} = h_{e-sh}A_{sh,out}(T_{amb} - T_{sh}) \tag{3}$$

$$Q_{m-sh} = \sigma A_m F_{m-sh}(T_m^4 - T_{sh}^4) \tag{4}$$

$$Q_{a-sh} = h_{a-sh}A_{sh,in}(T_{cab} - T_{sh}) \tag{5}$$

where m_{sh} and c_{sh} represent the total mass and specific heat capacity of the cabin shell, respectively. In the solar radiation equation, α_{sh} is the absorptivity of the cabin shell, which depends on the material of the shell and the color intensity. Black vehicles have higher absorptivity, while white vehicles have lower absorptivity. In this study, a gray vehicle with moderate absorptivity is assumed, thus α_{sh} is set to 0.5. $A_{rad,sh}$ is the area of the outer surfaces which are illuminated by the sun, notably, window area is excluded, while I_{dir} and I_{diff} are the direct and diffused solar radiation intensity. Heat exchange between the cabin shell and internal mass is also radiation, with A_m and F_{m-sh} represent the internal mass surface area and the view factor. $A_{sh,in}$ and $A_{sh,in}$ are the inner and outer surface area of the shell including all the metal or plastic shell and the window glasses surface, and the convective heat transfer coefficient between the shell and cabin air h_{a-sh} is assumed to be constant because the inner air velocity is small enough to achieve free convection. When the vehicle is in driving, the convective heat transfer coefficient between the shell and ambient air h_{a-sh} will change rapidly due to the speed change, which can be shown as an empirical formula:[33]

$$h_{e-sh} = 1.163(4+12\sqrt{v}) \tag{6}$$

where the unit of v is m/s.

Internal mass: One of the specific characteristics of the cabin thermal load is that the large windows allow solar radiation to pass directly through the glass and heat the internal mass, which is especially significant in the summer, resulting in a rapid temperature rise in the cabin and significant thermal load.[34] For the internal mass model, in addition to solar radiation $Q_{sol,m}$, the other thermal loads include radiation with the cabin shell Q_{sh-m} and convection with the cabin air Q_{a-m} The governing equations of internal mass model are as follows:

$$m_m c_m \frac{dT_m}{dt} = Q_{sol,m} + Q_{a-m} + Q_{sh-m} \tag{7}$$

$$Q_{sol,m} = \alpha_m \tau_w (I_{dir} + I_{dif}) A_w \tag{8}$$

$$Q_{a-m} = h_{a-m} A_{a-m} (T_m - T_{cab}) \tag{9}$$

where α_m is the absorptivity of the internal mass. Additionally, the solar radiation entering the cabin through the windows depends on the transmissivity of the window glass. According to the study,[35] the transmittance value τ_w is 0.45. A_w is the window surface area, calculated based on the geometric dimension of the Tesla Model 3.

Cabin air: The cabin thermal load is the largest source of demand for the TMS, determining the energy output and consumption required by the heat pump system during operation. The air inside the cabin is the direct target of the cabin TMS, and changes in cabin air temperature directly affect the thermal comfort of the driver and passengers. External thermal loads acting on the cabin shell and internal components ultimately lead to increases or decreases in cabin air temperature. In the cabin environment, the thermal load is managed by blowing air into the interior via the evaporator (in summer) or the condenser (in winter) using fans, which remove the thermal load generated inside the cabin, include heat exchange with the cabin shell Q_{sh-a}, heat exchange with the internal mass Q_{m-a}, heat dissipation from occupants Q_{occ}, heat generated by electronic devices inside the vehicle Q_{elec} and the ventilation load. These factors collectively influence the cabin air temperature, creating a dynamic thermal environment that the TMS must effectively regulate to maintain comfort and energy efficiency. This comprehensive modeling approach ensures that all significant heat sources and sinks are accounted for, providing a robust foundation for optimizing the TMS in electric vehicles. The governing equations of cabin air model are as follows:

$$m_{air} c_{air} \frac{dT_{cab}}{dt} = Q_{cab} + \dot{m}_{a,sup} c_{air} (T_{a,sup} - T_r) \tag{10}$$

$$Q_{cab} = Q_{sh-a} + Q_{m-a} + Q_{occ} + Q_{elec} + Q_{vent} \tag{11}$$

where $\dot{m}_{a,sup}$ is the airflow rate (mass flow rate) provided by the air conditioning system. $T_{a,sup}$ is the supply air temperature and T_r is the return air temperature, which is the cabin air temperature. Because the metabolic heat production rates of the driver and passengers differ,[36] the heat dissipation values are 150W for the driver and 100W for the passengers. The heat generated by the electronic devices inside the vehicle is a fixed value of 150W.[25] The ventilation rate is primarily set to introduce an appropriate amount of fresh air, creating an indoor air quality (IAQ) that meets safety and comfort standards for passengers in the cabin. In a long-term enclosed vehicle environment, the concentration of carbon dioxide and other pollutants can rise rapidly. The introduction of fresh air effectively reduces the concentration of these gases or particulates. The standard for fresh air volume is set at 3.6 L/s per person to ensure driving safety.[37] To ensure the thermal comfort of the occupants, the cabin temperature is set to 25°C., a PID controller is adopted for controlling the supply air mass flow rate to maintain the cabin air temperature at setpoint.

Battery package. The Tesla Model 3 utilizes 2170(cylindrical cells with a diameter of 21mm and a height of 70mm) lithium-ion battery cells.[38] The Standard Range version of Model 3 consists of a total of 2976 cells, each with a nominal voltage of 3.7V, forming the battery pack. In the package, every 31 cells form a brick, and then grouped into four modules, two of which contain 25 bricks each, and the other two contain 23 bricks each. These modules are connected in series to provide the vehicle with a nominal voltage exceeding 350V and a total capacity of 60kWh. When charging and discharging, the internal resistance of the batteries causes heat generation Q_{bat} according to Bernardi's theory.[39] The amount of heat generated depends on the current charge and discharge power of the batteries. In the Tesla Model 3, the battery pack is positioned in the vehicle's chassis. The bottom of the pack is encased by the chassis, while the top is in direct contact with the air within the chassis, resulting in convective heat transfer $Q_{bat,air}$ between the battery cell and the environment. For the battery thermal management system (BTMS), a 50% concentration ethylene glycol solution is used as the coolant.[25] The ethylene glycol pipelines run parallel through each module, contacting the sides of the batteries to cool down or heat up of the battery pack. The battery thermal management is calculated as follows:

$$m_{bat} c_{bat} \frac{dT_{bat}}{dt} = Q_{bat} + Q_{bat,air} + \dot{m}_{batcool} c_{cool} (T_{batcoolin} - T_{batcoolout}) \tag{12}$$

$$Q_{bat} = N_{cell} (I_{cell}{}^2 R_{cell} - I T_{bat} \frac{dU_{OC}}{dT_{bat}}) \tag{13}$$

$$I_{cell} = \frac{P_{bat}}{N_{cell} V_{cell}} \tag{14}$$

$$Q_{bat,air} = h_{bat,air} A_{bat,air} (T_{amb} - T_{bat}) \tag{15}$$

$$\dot{m}_{batcool} c_{cool} (T_{batcoolout} - T_{batcoolin}) = h_{bat,cool} A_{bat,cool} \Delta T_{lm} \tag{16}$$

where $\dot{m}_{batcool}$ is the battery coolant mass flow rate, $T_{batcoolin}$ and $T_{batcoolout}$ are the inlet and outlet temperature of the coolant. N_{cell} is the total number of battery cells, R_{cell} and V_{cell} is the internal resistance and the nominal voltage of each battery cell and P_{bat} is the absolute value of battery charging of discharging power, U_{OC} is the open circuit voltage and dU_{OC}/dT_{bat} represents the entropy coefficient of the battery. The airflow speed within the vehicle chassis is low, thus the convective heat transfer between the battery and the environment is approximated as natural convection. The convective heat transfer coefficient $h_{bat,air}$ is set according to the calculations reported in previous investigation,[40] and $A_{bat,air}$ is the total bottom area of the battery package. For each battery cell, 1/6 of the side area contacts the coolant plate, and ΔT_{lm} is the Logarithmic mean temperature difference (LMTD) between the battery and coolant, calculated as $\Delta T_{lm} = \frac{\Delta T_1 - \Delta T_2}{\ln \frac{\Delta T_1}{\Delta T_2}}$, where ΔT_1 and ΔT_2 are the temperature differences at coolant inlet and outlet.

For the battery package, excessively high temperatures can pose a risk of thermal runaway and potential self-ignition, while low temperatures can reduce ion activity within the battery, significantly increasing internal resistance and impacting battery efficiency.[41] According to research findings, the optimal operating temperature for the battery is also around 25°C.[7] Another PID controller is also adopted for controlling the battery coolant mass flow rate to keep the battery temperature. Parameters of battery thermal management model are given in Table S2.[25,40,42]

Electric motor. The electric motor is also a significant thermal load source in the thermal management system. The heat generated by the motor Q_{mot} comes from frictional heating during operation. Motor efficiency depends on the current speed and torque of the motor.[40] In the electric motor thermal management model of this study, the same coolant used for the battery is employed to cool the motor. The contact area between the motor and the ambient air is almost negligible, so all the heat generated by the motor is carried away by the coolant. Since motor efficiency and safety is not sensitive to the temperature, the motor temperature setpoint is set to 75°C, which is significantly higher than the ambient temperature in any season throughout the year. Therefore, a radiator is used to directly dissipate the motor heat to the outside environment. The motor thermal management is calculated as follows:

$$m_{mot}c_{mot}\frac{dT_{mot}}{dt} = Q_{mot} + \dot{m}_{motcool}c_{cool}(T_{motcoolin} - T_{motcoolout}) \tag{17}$$

$$Q_{mot} = P_{mot,in} - P_{mot,out} \tag{18}$$

$$\dot{m}_{motcool}c_{cool}(T_{motcoolout} - T_{motcoolin}) = h_{mot,cool}A_{mot,cool}\Delta T_{lm} \tag{19}$$

In the radiator:

$$\dot{m}_{radair}c_{air}\,(T_{airout} - T_{amb}) = h_{rad,air}A_{rad}\Delta T_{lm} = \dot{m}_{motcool}c_{cool}(T_{motcoolout} - T_{motcoolin}) \tag{20}$$

where $P_{mot,in}$ and $P_{mot,out}$ are the power input and output of the motor, which can be simulated by the powertrain model in FASTSim. The full circle for the motor coolant first takes heat from the motor and then exhausts it to the outdoor air by the radiator. Parameters of motor thermal management model can be found in Table S3.

Heat pump system

The heat pump system model simulates a complete vapor compression refrigeration cycle, using R134a as the refrigerant. The main components of the heat pump system model include a compressor, condenser, electronic expansion valve, and evaporator. During the vapor compression cycle, the refrigerant first undergoes isentropic compression in the compressor, then flows through the condenser, where it releases heat to the outside, transitioning from gas to liquid. The refrigerant then passes through the electronic expansion valve for adiabatic expansion, resulting in a sharp decrease in temperature and pressure. Next, it enters the evaporator, where it absorbs heat and evaporates back into gas. Finally, the gaseous refrigerant returns to the compressor to complete the cycle. The switch between cooling and heating modes is achieved by reversing the refrigerant flow direction using a four-way valve. To ensure complete condensation in the condenser and complete evaporation in the evaporator, the simulation sets a subcooling degree of -5°C for the condenser and a superheating degree of 5°C for the evaporator.

Compressor: The compressor model is calculated as follows:[25]

$$N_{comp} = \frac{\dot{m}_{rfg}\rho_{rfg}10^3}{60\eta_{vol}V_{comp}} \tag{21}$$

$$P_{comp} = \frac{\dot{m}_{rfg}(h_{compout} - h_{compin})}{\eta_{is}} \tag{22}$$

$$\eta_{is} = a_1 + a_2\frac{p_{compout}}{p_{compin}} + \left(a_1 + a_2\frac{p_{compout}}{p_{compin}}\right)N_{comp} + \left(a_1 + a_2\frac{p_{compout}}{p_{compin}}\right)N_{comp}^2 \tag{23}$$

$$\eta_{vol} = b_1 + b_2\frac{p_{compout}}{p_{compin}} + \left(b_1 + b_2\frac{p_{compout}}{p_{compin}}\right)N_{comp} + \left(b_1 + b_2\frac{p_{compout}}{p_{compin}}\right)N_{comp}^2 \tag{24}$$

where $\dot{m}_{rfg}$ is the mass flow rate of the refrigerant, ρ_{rfg} is the refrigerant density at the compressor entrance, h_{compin} and $h_{compout}$ represent refrigerant enthalpy before and after compression. The inlet and outlet pressure are set to 2 Bar and 14 Bar, respectively.

Condenser/ Heat exchanger: In heating mode, the condenser supplies heat to the return air in the cabin, and the heat transfer in the condenser is given as follows:

$$\dot{m}_{rfg}(h_{compout} - h_{condout}) = h_{cond}A_{cond}\Delta T_{lm} = \dot{m}_{air}c_{air}(T_{airout} - T_{airin}) \tag{25}$$

Expansion valve: Adiabatic expansion is performed in the expansion valve, so the outlet enthalpy h_{exout} remains the same as $h_{condout}$.

Evaporator/ Heat exchanger: In cooling mode, the evaporator functions to provide cooling to the cabin or the battery. The heat transfer in the evaporator is calculated as follows:

$$\dot{m}_{rfg}(h_{evapout} - h_{evapin}) = h_{evap}A_{evap}\Delta T_{lm} = \dot{m}_{air}c_{air}(T_{airout} - T_{airin}) \tag{26}$$

Notably, the right side of equation (27) depends on the fluid type in the other side of evaporator/ heat exchanger, when heat exchanger is cooling the battery, the fluid is the ethylene glycol coolant.

Operating mode definition

Summer: Under summer conditions, intense solar radiation and high outdoor temperatures can cause the cabin temperature to rise rapidly, while the ambient temperature is also significantly higher than the set temperature of the battery pack. Therefore, during summer, the heat pump system operates in a mixed cooling mode, as shown in Figure 1B. The R134a refrigerant circuit is required to simultaneously cool both the cabin and the glycol coolant for the battery pack. After leaving the expansion valve, the refrigerant is directed through a three-way valve, which controls its flow to the cabin cooling evaporator and the heat exchanger connected to the battery coolant loop, where independent evaporation processes occur. Since the operating temperature range of the electric motor is broader, an independent glycol cooling loop is used to discharge waste heat to the ambient environment via a radiator. In addition to temperature control for the cabin, battery pack, and motor, two PID controllers are employed to regulate the subcooling of the refrigerant in the condenser and the superheating of the refrigerant in the evaporator, thereby preventing liquid slugging in the compressor and improving the overall system efficiency.

Winter: Under winter operating conditions, the heat pump is switched to heating mode by reversing the four-way valve to provide thermal comfort for the cabin. However, for a cold-start vehicle, the initial temperatures of the cabin, battery pack, and motor are all close to the ambient temperature. While the cabin temperature can be quickly raised through the operation of the heat pump, the self-heating of the battery pack is insufficient to bring its temperature to the optimal working range within a short time. Therefore, a PTC heater is added to the glycol cooling loop of the battery to preheat it during the early stages of driving. The vehicle cabin is heated by a heat pump system equipped with WHR, as shown in Figure 1C.

Model validation

All models are developed using the programming language Python, version 3.9. The powertrain model is coupled with the TMS model developed as described previously. The coupled model outputs include vehicle speed, battery charge/discharge power, motor power, driving distance, state of charge (SOC), as well as cabin air temperature, airflow parameters, refrigerant loop status, and TMS energy consumption.

To validate the accuracy of the cabin heat transfer model developed in this study, simulation data is compared with experimental results of the temperature rise in a parked vehicle in summer in a validated paper.[35] Simulations are conducted under identical environmental conditions to those in the experiment, which took place from 9:45 AM to 1:15 PM on a summer day in Spain. The solar radiation intensity and outdoor temperature on the day of the experiment are according to the validated data.[35] The vehicle used in the experiment was a vehicle with almost equivalent size to the Tesla Model 3 used in this study. 7 temperature sensors were placed inside the vehicle to measure air temperature changes in different cabin areas as shown in Figure 2A. Among the results, the temperatures recorded by sensors 5 and 6 were the closest to their simulation results. Therefore, this study compares the simulation results with the measurements from sensors 5 and 6, as shown in Figure 2B. From the comparison in the figure, it is evident that the simulation results from the model developed in this study show good agreement with the experimental results, especially closely matching the temperature variation curve of sensor 5. Under the given environmental conditions, the cabin air temperature increased from an initial 25.5°C to approximately 50°C, which

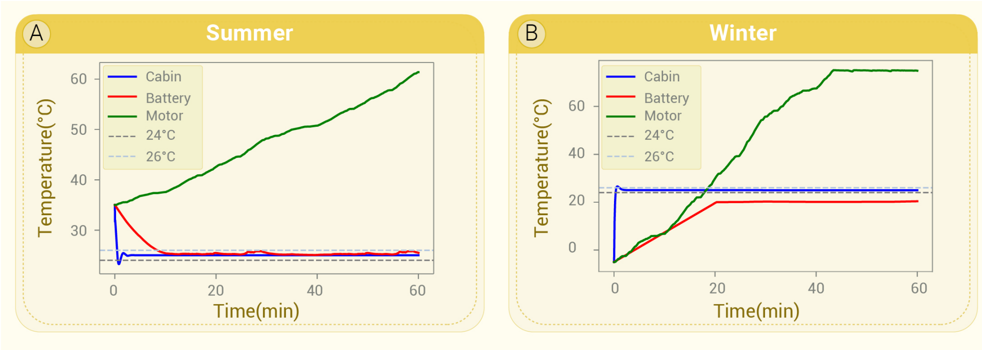

Figure 3. Temperature simulation results. (A) Ambient temperature 35℃ in summer. (B) Ambient temperature -5℃ in winer.

indicates that even in conditions where the outdoor temperature is not extremely high, solar radiation can lead to a rapid rise in the interior temperature of the vehicle.

The heat pump system was also validated in a laboratory setting. The experimental setup utilized a small-scale heat pump system based on a Midea 31CC compressor, with a rated cooling capacity of 2000 W, which is close to the cabin cooling load in this study. A total of 89 experimental simulations were conducted under varying conditions of evaporation pressure, condensation pressure, compressor suction temperature, and refrigerant enthalpy. The experimental results were compared with the heat pump model established in this study, as shown in Figure 2 C–H. Four parameters were compared: refrigerant mass flow rate, condensation temperature, refrigerant outlet enthalpy, and compressor power. It can be clearly observed from the figures that the model shows a high degree of agreement with the experimental results, with the errors of all four parameters within an acceptable range.

Driving range assessment with TMS: results and analysis

To ensure that the research results accurately reflect most driving scenarios, this study adopts the World Light Vehicle Test Procedure (WLTP) as the simulation scenario for the vehicle powertrain and TMS. The duration of a single WLTP cycle is 1800 seconds, corresponding to typical urban, suburban, rural, and highway traffic conditions. To better observe the temperature and energy consumption simulation results, each simulation runs the WLTP cycle twice, resulting in a total simulation time of 3600 seconds per run. Under the default simulation conditions, the typical meteorological temperatures for summer and winter are 35°C and -5°C, respectively. A sensitivity analysis of different temperatures and other environmental parameters will be conducted in system power and driving range.

Thermal dynamics

The initial conditions for the simulation of cabin air temperature, battery pack temperature, and motor temperature were set to match the ambient temperature. The simulation results for temperature variations under typical summer and winter (pure heat pump mode with WHR off) conditions are shown in Figure 3 A & B, respectively. The results clearly indicate that, under the operation of the heat pump, the cabin air temperature stabilizes around the setpoint of 25°C approximately 2 minutes after the start of driving, in both summer and winter conditions. In summer, the cabin temperature initially drops to about 23°C before quickly rising to around 25°C. In winter, the cabin temperature initially exceeds 26°C during the first two minutes but then decreases to the setpoint. No significant overshoot is observed in either scenario, ensuring thermal comfort for passengers inside the cabin. This demonstrates that the PID controllers employed in this study are effective under the given boundary conditions.

The simulation results for battery temperature are also shown in the figures as red curves. According to Equation (13) and (14), the heat generation of the battery is related to its charging or discharging power. During the WLTP cycle, the vehicle undergoes multiple acceleration and deceleration events. During acceleration, the battery consumes energy to provide mechanical power to the vehicle, overcome rolling resistance, air drag, and supply energy to auxiliary systems. During deceleration, regenerative braking recharges the battery. In summer, the initial battery temperature is higher than the setpoint and is quickly cooled by the heat pump, reaching the setpoint of approximately 25°C within about 10 minutes. As the vehicle operates, the battery's heat generation fluctuates with its discharging and charging power, leading to temperature variations throughout the simulation. The summer simulation results show that the battery temperature tracking error remains within ±1°C, meeting the requirements for battery efficiency and safety management. In winter, the initial battery temperature is significantly lower than the setpoint. To ensure the battery temperature quickly reaches the operational range, a PTC heater is first used to preheat the battery to 20°C. Subsequently, the battery's own heat generation gradually brings its temperature closer to the setpoint.

The green curves in the figures represent the motor temperature variations. From the results, it can be observed that, since the motor's operational temperature tolerance is much higher than the ambient temperature, the motor temperature remains well within the maximum allowable range during a single simulation, regardless of whether it is summer or winter. Therefore, motor cooling is not required during this process.

Cabin thermal load

The cabin thermal load corresponds directly to the calculations presented in thermal load, including contributions from the vehicle cabin shell, interior objects, passenger metabolism, ventilation, and equipment heat generation. The simulation results are shown in Figure 4. In summer and winter, cooling and heating are required, respectively, resulting in opposite load signs. To enhance the clarity of the figure, the load values for winter have been adjusted by reversing their signs.

As shown in the figure, regardless of the season, the load from the cabin shell accounts for the largest proportion of the total load, which is particularly evident in winter, where it exceeds 80%. According to the calculations of cabin shell temperature in thermal load, this load mainly originates from two components: solar radiation and convective heat exchange with the environment. Solar radiation raises the shell temperature, while convective heat exchange lowers it. In summer, the effect of solar radiation is significant, and its heating effect outweighs the cooling effect of convection, resulting in a cooling load for the cabin air. In winter, solar radiation is weak, and the heat loss from convection far exceeds the heat gain from absorption, creating a heating load for the cabin.

Under intense summer sunlight, interior objects in the cabin, such as dark leather seats, rapidly heat up, often exceeding the cabin air temperature, further increasing the cooling demand. In winter, the situation is reversed. Under the default simulation conditions, there are no passengers in the vehicle apart from the driver, so the contribution of passenger metabolism and ventilation loads is relatively small. In winter, the heat generated by passenger metabolism and equipment reduces the burden on the heat pump system. However, an increase in the number of passengers will increase the system's ventilation demand. The impact of passenger numbers on system load depends on the difference between the cabin temperature setpoint and the ambient temperature.

System power and driving range

In this study, the energy consumption of the vehicle TMS includes the compressor, various fans, and pumps, as well as the PTC heater for rapid battery heating in winter. The fans include those for the condenser, evaporator, and radiator, while the pumps are placed in the glycol coolant circuits for the motor and battery. The energy consumption simulation results under default environmental conditions are shown in Figure 5. In winter, due to the battery's temperature requirements, the average energy consumption of TMS is significantly higher than in summer during a single simulation. Additionally, the PTC heater's average energy consumption accounts for more than 65% of the total, representing a heavy burden on the system. In summer, under an

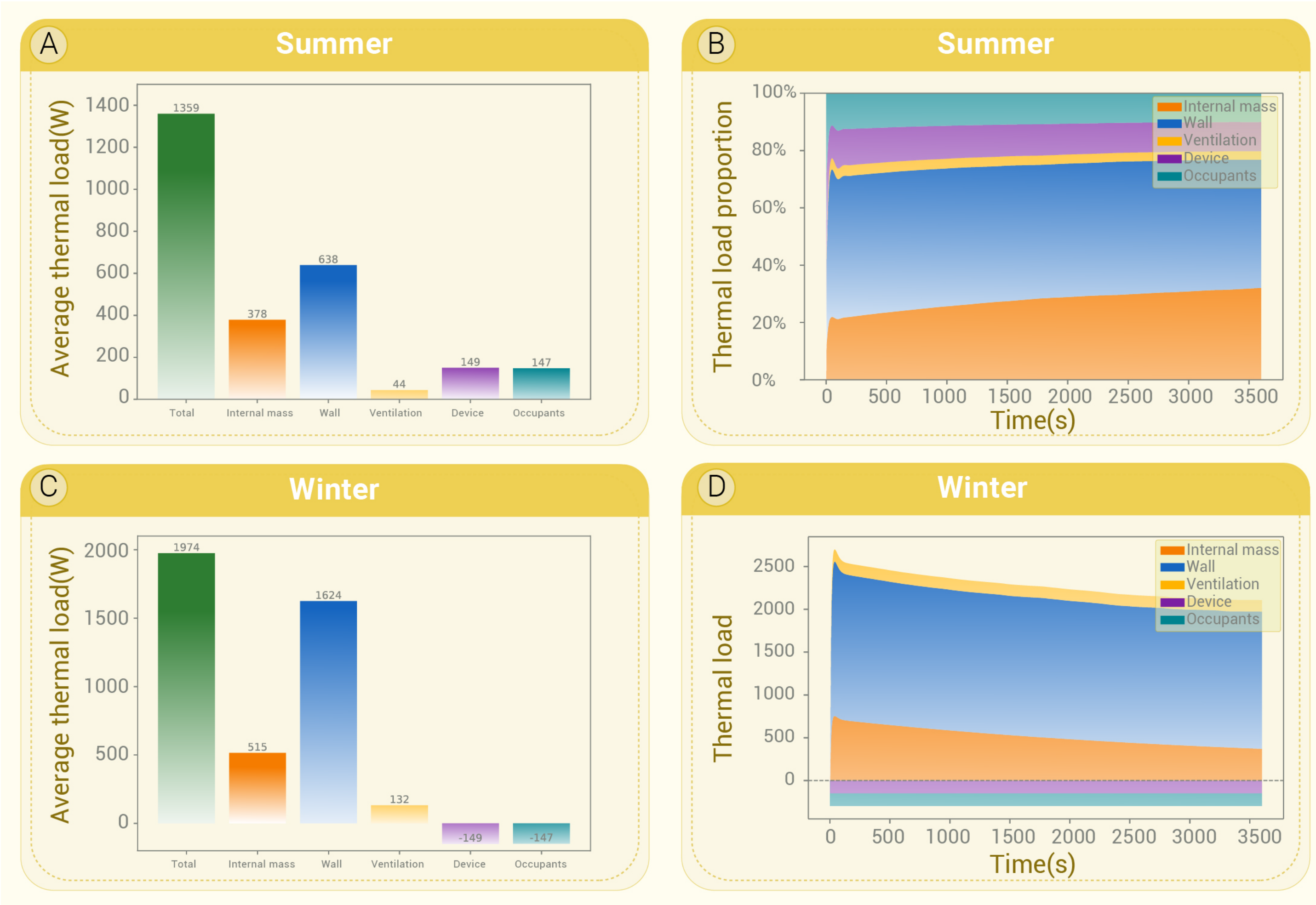

Figure 4. Thermal load. (A) Value in summer, (B) percentage in summer, (C) value in winer, (D) percentage in winter.

outdoor temperature of 35°C, the system's overall energy consumption exceeds 1200 W, with the compressor being the largest source of energy consumption, accounting for more than 60%. Since the radiator fans for the battery and motor do not need to operate in this scenario, their energy consumption is 0. The pump energy consumption in the refrigerant circuit mainly comes from the battery. The average compressor power in summer is higher than in winter because both the cabin and the battery require cooling through the heat pump system. In winter, the power of the cabin fan is significantly higher than in summer because the cabin load is larger, increasing the demand for air circulation. The impact of enabling TMS functions on driving range under different climate conditions is shown in Figure 5B. Without using TMS, the vehicle's standard driving range is 327.99 miles. When TMS is activated, the driving range decreases by 12.25% in summer and 25.43% in winter under standard operating conditions, corresponding to reductions of over 40 and 80 miles, respectively.

Parametric sensitivity analysis

This section explores the impact of various boundary conditions, such as environmental factors, vehicle parameters, and the number of occupants, on system energy consumption and driving range. Since cabin thermal load is the largest source of energy consumption for the TMS, environmental factors and internal/external heat sources ultimately affect the range by altering the cabin thermal load. Under the simulation cycle used in this study, parameters such as solar radiation intensity, ambient temperature, number of occupants, and even vehicle body color can quantitatively influence the vehicle's driving range. A single-factor sensitivity analysis is used to quantitatively examine the range variations caused by these factors. The reference conditions for summer are as follows: an outdoor temperature of 35°C, direct solar radiation intensity of 800 W/m^2, one driver in the vehicle, body absorption rate of 0.5, and window transmittance of 0.5. In winter, the typical meteorological conditions are an outdoor temperature of -5°C, no direct solar radiation, and the diffuse radiation intensity of 200 W/m^2. By keeping all other conditions constant, each parameter is varied individually to calculate new energy consumption and driving range results. The simulation results for summer and winter are shown in Figure 6, respectively. The adjustable parameters in summer include ambient temperature, window transmittance, body absorption rate, and number of passengers. In winter, due to low solar radiation intensity, only ambient temperature and the number of passengers are adjusted.

From Figure 6A & B, it is evident that as ambient temperature increases, the energy consumption of TMS rises significantly. For every 5°C increase in ambient temperature, energy consumption increases by approximately 250 W. The cabin shell load has the greatest impact on thermal load, as higher ambient temperatures suppress the convective heat dissipation from the cabin shell to the environment. When ambient temperature rises above a certain threshold, this heat transfer process reverses, and the cabin begins to absorb more heat from the environment. When the ambient temperature increases from 30°C to 40°C, the driving range decreases by over 8%, equivalent to approximately 25 miles. Increasing window transmittance and body absorption rates also intensifies the heat transfer process from solar radiation into the cabin. However, from the perspective of overall energy consumption, the impact is not as significant as that of increasing ambient temperature. When window transmittance increases from 0.2 to 0.8, the driving range decreases by only 1.42%, or about 4 miles. In summer, increasing the number of passengers also leads to a notable rise in TMS energy consumption. Adding two passengers increases the system's average energy consumption by approximately 100 W and reduces the range by about 5 miles, which is caused by the combined effects of passenger metabolic heat generation and increased ventilation load.

In winter, a decrease in ambient temperature results in a more severe

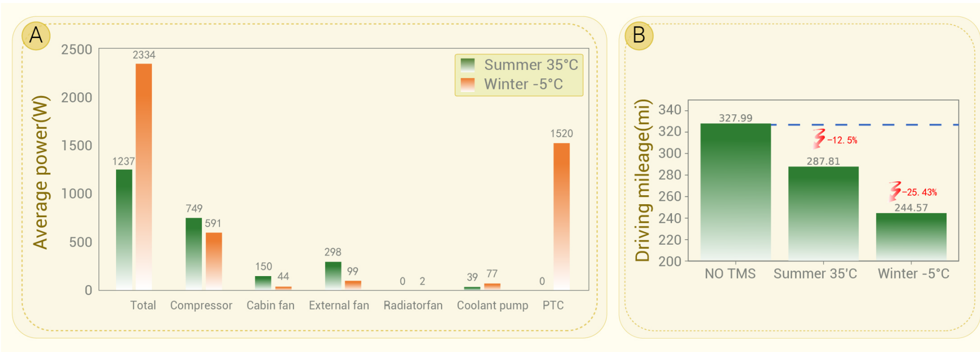

Figure 5. System power simulation results. (A) TMS energy consumption in typical summer and winter conditions. (B) Driving range degradation.

reduction in driving range. From Figure 6 I & J, when ambient temperature drops from 0°C to -10°C, the overall energy consumption of TMS increases by approximately 700 W. The most significant contributor to this increase is the convective heat exchange load between the cabin shell and the environment. Starting from 0°C, for every 5°C decrease in ambient temperature, the vehicle's driving range decreases by more than 8%. The range difference between 0°C and -10°C is approximately 36 miles. In winter, increasing the number of passengers has a smaller impact on reducing driving range compared to summer, adding two passengers reduces the range by only about 0.4% because more passengers contribute heat to the cabin, partially offsetting the heat demand on the heat pump system.

MATERIALS AND METHODS

WHR mode definition

The heat generated by the electric motor during one simulation cycle is shown in Supplementary Information, with the highest value reaching over 2000W, and the average thermal load for the motor is 694W.

To compare the impact of different WHR strategies on energy consumption and driving range, this study defines three mutually exclusive operating modes:

S0: Pure Air-Source Heat Pump (Baseline, no WHR)

Mechanism: On the evaporator side, the refrigerant exchanges heat solely with the outdoor evaporator and does not flow through the motor cooling circuit. Cabin and battery thermal demands are met entirely by the air-source heat pump. Motor waste heat is rejected to the ambient environment via the radiator.

Physical Principle: The evaporation temperature is predominantly governed by ambient temperature and airflow rate. Lower ambient temperatures lead to decreased evaporation pressure, increased compressor pressure ratio, and consequently, higher system power consumption. S0 serves as the control case for quantifying the marginal benefits of introducing WHR.

S1: Pure WHR (Hysteresis-based On-Off Recovery)

Mechanism: Following a cold start, the heat pump initially extracts heat from the ambient air. When the motor temperature exceeds the upper threshold (T_{on}), a three-way valve diverts the refrigerant flow through the heat exchanger in the motor cooling circuit for heat recovery. Recovery ceases, and ambient heat extraction resumes, when the motor temperature falls below the lower threshold (T_{off}). A minimum hysteresis band (ΔT_{min}) is implemented to prevent frequent switching.

Physical Principle: During recovery phases, the evaporator-side temperature level increases, reducing the compressor pressure ratio and fan power consumption. However, continuous heat extraction from the motor affects its warm-up rate and the subsequent temperature level available for recovery. The thresholds T_{on} and T_{off} govern the trade-off between recovery timing and duration.

S2: Dual-Source WHR (Parallel Dual-Heat-Source Recovery)

Mechanism: On the evaporator side, the refrigerant exchanges heat simultaneously and in parallel with both the outdoor evaporator and the motor cooling circuit heat exchanger. The heat absorption rate from the motor circuit is continuously regulated via electronic expansion valves (EEVs), adjusting the refrigerant mass flow rate or the effective heat exchange capacity. In this study, the absorbed heat power from the motor circuit is uniformly denoted as Q_{whr} for optimization and analysis purposes, which is functionally equivalent to a distribution coefficient φ ∈ [0,1].

Physical Principle: Increasing Q_{whr} instantaneously elevates the evaporation temperature, reducing the pressure ratio and system power consumption. However, this suppresses the motor's own temperature rise, potentially diminishing the subsequent temperature level available for recovery and its duration. Conversely, a low Q_{whr} has the opposite effect. This mode embodies the trade-off between instantaneous efficiency and cumulative recoverable energy.

Methodology

Genetic algorithm (GA) is a derivative-free, population-based global optimization method inspired by an abstraction of natural selection and genetic mechanisms. It maintains a population of multiple candidate solutions (individuals) within the parameter space. Through iterative cycles of selection, crossover, mutation, and elitism preservation, the overall quality of the population is progressively improved, eventually converging towards an approximate global optimum within the feasible region. Specifically, the decision variables are encoded into gene strings using real numbers (in this study, the gene for S1 is a two-dimensional vector $[T_{on}, T_{off}]$, while for S2 it is a one-dimensional scalar $[Q_{whr}]$). The fitness of each individual is evaluated based on the average thermal management power $J(\theta)$ obtained from a single simulation run.

Selection: Favors individuals with higher fitness probabilistically, aiming to propagate "good genes" to the next generation.

Crossover: Recombines genetic material from two parent individuals to produce offspring, exploring combinations in the vicinity of current promising regions.

Mutation: Applies small random perturbations to genes, maintaining population diversity and aiding escape from local optima.

Elitism Preservation: Directly carries the best individual(s) over to the next generation unchanged, preventing performance degradation.

In scenarios characterized by non-convexity, non-differentiability, and objectives accessible only via black-box simulation, GA offers significant advantages. It requires no gradient information and facilitates parallel evaluation. Consequently, GA can robustly approximate deployable near-optimal strategy parameters within a limited computational budget.

GA-based optimization setup

Decision variables

$$S1 : \theta_{S1} = [T_{on}, T_{off}]$$

$$S2 : \theta_{S2} = [Q_{whr}]$$

Objective function and fitness measurement

Optimization objective for one single simulation cycle is the minimal TMS average power consumption, which can be referred to as:

$$S1\&2 : J(\theta) = (1/\tau)\int_{0}^{\tau} P_{tms}(t;\theta)dt$$

The fitness is based on J(θ), but if there is a constraint violation, the penalty is adopted as:

$$S1\&2 : \widehat{J}(\theta) = J(\theta) + \sum k\lambda_k max(0, g_k(\theta))$$

Where λ_k is the penalty coefficient of each constraint term.

Constraints

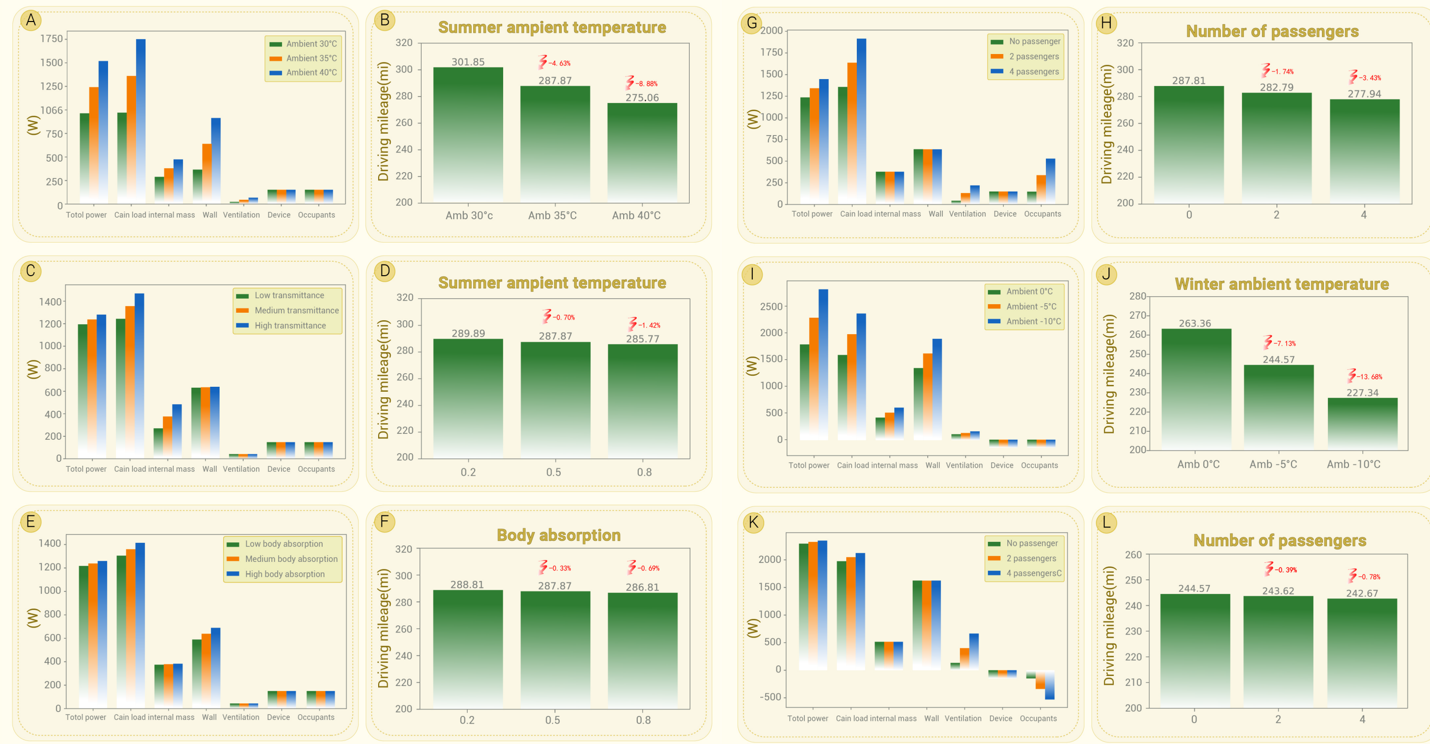

Figure 6. Sensitivity analysis of total power consumption, thermal load and driving mileage in summer and winter. (A) & (B) Ambient temperature. (C) & (D) Window transmittance. (E) & (F) Cabin shell absorption. (G) & (H) Number of passengers. (I) & (J) Ambient temperature. (K) & (L) Number of passengers.

For the S1 mode, the hard constraints on T_{on} and T_{off} must lie within the permissible motor temperature range. Specifically, they must not exceed the maximum motor control temperature of 75 °C and not fall below the ambient temperature. To prevent frequent cycling of the heat recovery mode caused by an insufficient difference between T_{on} and T_{off}, a minimum hysteresis band is imposed by setting T_{on} to be at least 3 °C higher than T_{off}. For the S2 mode, Q_{whr} must be constrained within a suitable power range. Its upper limit is set to 700 W, representing the average motor heat generation during a single simulation. Conversely, a very low Q_{whr} (implying minimal refrigerant flow) can lead to significant system oscillations during simulation. Therefore, a lower limit of 100 W is specified for Q_{whr}. Based on the principles above, the constraints for the control variables are defined as follows:

$$S1: T_{on} \in [T_{amb}+3, T_{ref}], T_{off} \in [T_{amb}, T_{on}-3]$$

$$S2: Q_{whr} \in [100{,}700]\,W$$

RESULTS AND DISCUSSIONS

The GA configurations detailed in methodology were applied to optimize the S1 and S2 WHR modes. The optimization process were implemented using the eaSimple algorithm within the DEAP framework, with a population size of 50, 40 generations, a crossover probability of 70%, and a mutation probability of 20%. Fuzzy crossover and tournament selection (selTournament) were employed. The optimization was performed on a desktop computer equipped with 32 GB of RAM, an i5-13600KF processor, and an NVIDIA 4060Ti graphics card with 16 GB of VRAM. The total computation time for a complete optimization under a single operating condition was approximately 8000 seconds.

Optimization was conducted for both S1 and S2 WHR modes under a typical winter condition (ambient temperature of -5 °C). The optimal parameters were calculated as T_{on} = 63.2 °C and T_{off} = 11.4 °C for the S1 mode, and an optimal Q_{whr} = 402.6 W for the S2 mode. The corresponding system energy consumption is illustrated in Figure 7A. The total energy consumption of the heat pump system shown in the figure excludes the PTC heating energy consumption of the battery. The average energy consumption values for the S0, S1, and S2 heat pump systems are 772.9 W, 649.0 W, and 704.3 W, respectively. Compared to the baseline case without WHR (S0), the two WHR modes reduced system energy consumption by approximately 16% and 9%, respectively. As evident from the figure, the compressor power consumption decreases most significantly under the S1-Pure-WHR mode. However, the power consumption of the coolant circuit pump increases due to the higher flow rate of the ethylene glycol solution in the motor loop when WHR is active. In the S2-Dual-source mode, the compressor power consumption also decreases slightly, and the coolant pump power consumption is lower than that in S1. Nonetheless, the overall energy-saving effect of S2 is less pronounced than that of S1. Figure 7B shows the variation in driving range across different WHR modes. Due to the reduction in TMS energy consumption, the driving range increases under both WHR modes, by 1.8% and 1.0%, corresponding to approximately 4.5 miles and 2.5 miles, respectively. This improvement is not particularly significant primarily because, for each simulated drive cycle, the battery undergoes a heating process from the ambient temperature to its setpoint temperature. The PTC heating energy consumption for the battery constitutes a major portion of the total winter TMS energy consumption. The reduction in cabin thermal management energy consumption achieved through WHR would have a more substantial impact on extending the driving range after the vehicle transitions from startup to steady-state driving.

Figure 7C presents the average heat pump system energy consumption resulting from different WHR power levels in the S2 mode. The figure clearly indicates that the total system power first decreases and then increases with rising WHR power, which aligns with the trade-off in recoverable heat quantity discussed previously. Figure 7D further summarizes the energy consumption optimization results and the optimal parameter combinations for the two WHR modes under different ambient temperatures defined in this study. For the S1 mode, T_{on} increases as the ambient temperature decreases, while T_{off} shows no clear trend. This is because, within a single simulation cycle, the system's initial WHR phase may not yet reach the lower motor temperature limit. A key finding is that for the pure WHR (S1) operation, the system prefers to initiate heat recovery only after the motor temperature has risen to a higher level and requires a sufficiently large difference between T_{on} and T_{off} to avoid frequent WHR cycling during a single drive cycle, thereby achieving lower total system energy consumption. For the S2 mode, the optimal heat recovery power (Q_{whr}) slightly increases as the temperature drops, but the change is not dramatic. This suggests that for the system, maintaining an appropriate heat absorption rate from the motor circuit is crucial. The

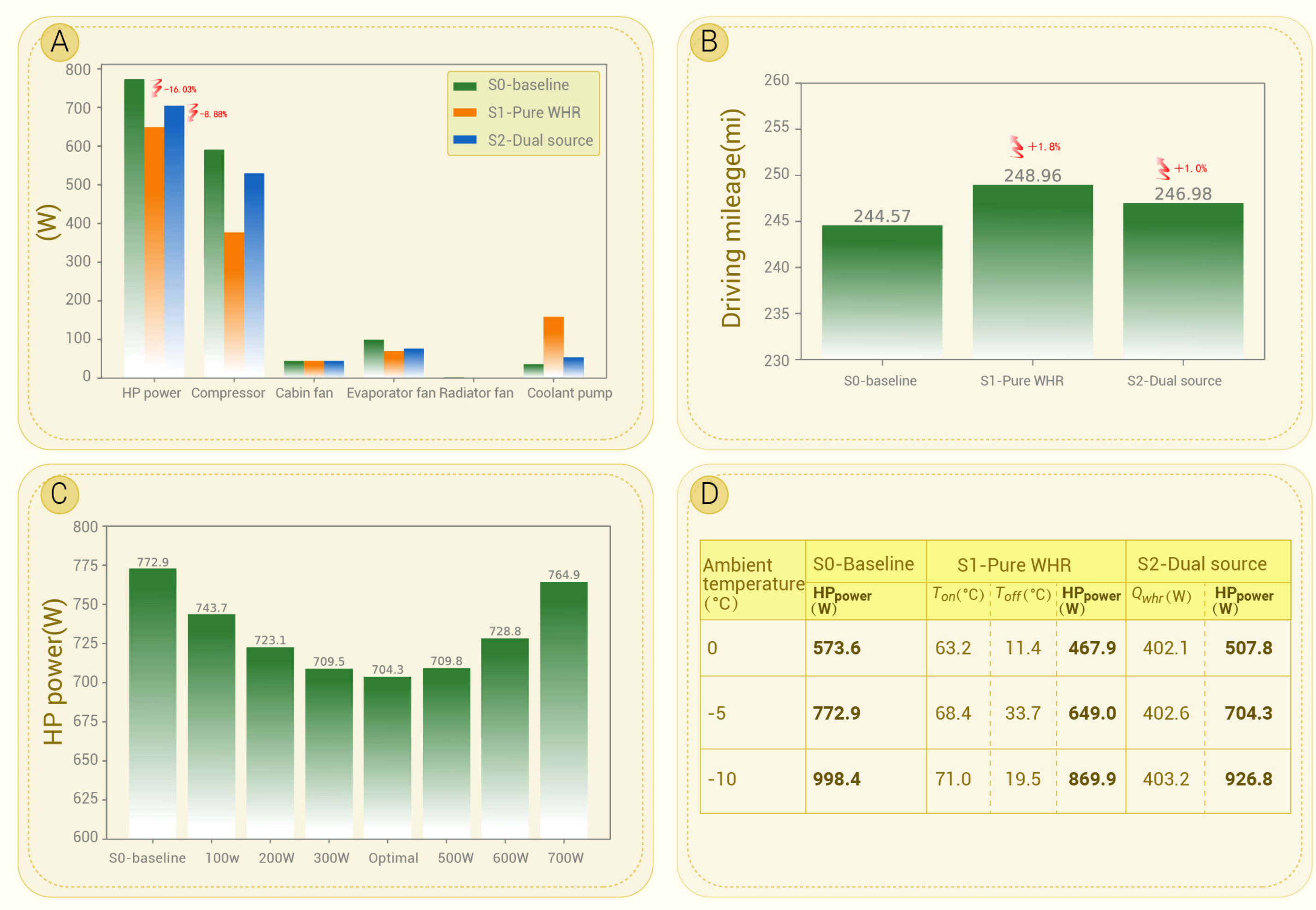

Ambient temperature (°C)	S0-Baseline	S1-Pure WHR			S2-Dual source	
	HP_{power} (W)	T_{on}(°C)	T_{off}(°C)	HP_{power} (W)	Q_{whr} (W)	HP_{power} (W)
0	**573.6**	63.2	11.4	**467.9**	402.1	**507.8**
-5	**772.9**	68.4	33.7	**649.0**	402.6	**704.3**
-10	**998.4**	71.0	19.5	**869.9**	403.2	**926.8**

Figure 7. Optimized WHR model. (A) Energy saving ratio of optimized WHR strategy. (B) Driving mileage extension of optimized WHR strategy. (C) Heat pump power consumption under different WHR intensity in S2. (D) Best WHR parameters under different environment conditions.

slight increase indicates that a lower ambient temperature necessitates ensuring a sufficient temperature difference for effective heat extraction from the motor circuit to maintain optimal system operation.

Based on the investigation of the two WHR modes in this study, the S1-Pure WHR mode demonstrates superior energy-saving performance, outperforming the S2-Dual-source mode across various ambient temperatures. From a system control complexity perspective, S1 also exhibits advantages over S2, as it does not require complex control of three-way valves to adjust refrigerant flow distribution between different circuits. Instead, it only necessitates simple on-off control within a specified temperature range. Furthermore, the application of the GA algorithm for optimizing WHR modes is highly significant. It avoids reliance on empirically defined heat recovery activation/deactivation temperatures and ensures the system can achieve optimal operation across varying environmental conditions.

CONCLUSION

Based on a plug-and-play, reusable vehicle-thermal management co-simulation platform, this study systematically evaluated the impact of the TMS on the energy consumption and driving range of electric vehicles and proposed and optimized two implementable strategies with motor waste heat recovery for winter conditions. The main conclusions are as follows:

1) The impact of the TMS on driving range is significant and seasonal: Under the WLTP dual-cycle conditions, activating the TMS resulted in a range reduction of approximately 12% to 16% in summer and 25% to 31% in winter. Cabin shell-related heat load is the dominant factor throughout the year, accounting for over 80% in winter and constituting the primary source of energy consumption for the heat pump system.

2) Range sensitivity to ambient and vehicle parameters is approximately linear: Ambient temperature is the most influential factor. The number of occupants, vehicle body absorptivity, and window glass transmittivity all exhibit nearly linear effects on range. For every 5°C increase in summer temperature, range decreases by approximately 4–8%; for every 5°C decrease in winter, range can drop by over 8%.

3) High proportion of battery PTC heating during warm-up limits the overall benefit of WHR in the cold-start phase: Although WHR effectively reduces heat pump power consumption, the energy consumed by battery PTC heating accounts for over half of the total during a single cold-start cycle, thereby limiting the potential improvement in overall vehicle range. The contribution of WHR to reducing system energy consumption becomes more pronounced during steady-state operation.

4) Optimality of WHR strategy depends on the trade-off between temperature level and duration. In the comparison of the three modes (S0, S1, S2) and the GA offline optimization results, S1 (on-off pure WHR) demonstrated superior overall energy savings compared to S2 (parallel dual-source). The optimal strategy for S1 tends to initiate heat recovery only after the motor temperature has risen to a sufficiently high level and maintains a wide enough hysteresis band (T_{on}/T_{off}) to reduce switching losses and disturbances. S2 exhibits a convex optimum regarding Q_{whr} reflecting the balance between the immediate benefit of increased evaporation temperature reducing pressure ratio and the long-term penalty of suppressed motor temperature rise leading to decreased subsequent recoverable temperature level and duration.

5) GA-based offline optimization provides robust and reusable basis for parameter tuning: This study identifies optimal value ranges and evolutionary trends for T_{on}/T_{off} in S1 and Q_{whr} in S2 across multiple ambient temperatures, providing a data foundation for establishing an engineering mapping from operational condition characteristics to strategy parameters.

REFERENCES

1. Liu W., Placke T. and Chau K.T. (2022). Overview of batteries and battery management for electric vehicles. *Energy Rep.* **8**:4058–4084. DOI:10.1016/j.egyr.2022.03.019
2. Li Y., Li X. and Jenn A. (2022). Evaluating the emission benefits of shared autonomous electric vehicle fleets: A case study in California. *Appl. Energy* **323**:119638. DOI:10.1016/j.apenergy.2022.119638
3. Xu Y., Zhang H., Yang Y., et al. (2023). Optimization of energy management strategy for extended range electric vehicles using multi-island genetic algorithm. *J. Energy Storage* **61**:106802. DOI:10.1016/j.est.2023.106802
4. Zhang G., Zou H., Qin F., et al. (2017). Investigation on an improved heat pump AC system with the view of return air utilization and anti-fogging for electric vehicles. *Appl. Therm. Eng.* **115**:726–735. DOI:10.1016/j.applthermaleng.2016.12.138
5. Vaz W., Nandi A.K.R., Landers R.G., et al. (2015). Electric vehicle range prediction for constant speed trip using multi-objective optimization. *J. Power Sources* **275**:435–446. DOI:10.1016/j.jpowsour.2014.11.093
6. Vatanparvar K., Faezi S., Burago I., et al. (2018). Extended range electric vehicle with driving behavior estimation in energy management. *IEEE Trans. Smart Grid* **10**:2959–2968. DOI:10.1109/TSG.2018.2799264
7. Zhao Y., Dan D., Zheng S., et al. (2023). A two-stage eco-cooling control strategy for electric vehicle thermal management system considering multi-source information fusion. *Energy* **267**:126606. DOI:10.1016/j.energy.2023.126606
8. Lahlou A., Ossart F., Boudard E., et al. (2018). A dynamic programming approach for thermal comfort control in electric vehicles. I*EEE Veh. Power Propuls. Conf. (VPPC)*:1–6. DOI:10.1109/VPPC.2018.8605022
9. Marshall G.J., Mahony C.P., Rhodes M.J., et al. (2019). Thermal management of vehicle cabins, external surfaces, and onboard electronics: An overview. *Engineering* **5**:954–969. DOI:10.1016/j.eng.2019.02.009
10. Zhou X., Lai D. and Chen Q. (2019). Experimental investigation of thermal comfort in a passenger car under driving conditions. *Build. Environ.* **149**:109–119. DOI:10.1016/j.buildenv.2018.12.022
11. Tsutsumi H., Hoda Y., Tanabe S.I., et al. (2007). Effect of car cabin environment on driver's comfort and fatigue. *SAE Trans.*:335–346. DOI:10.4271/2007-01-0444
12. Lei S., Xin S. and Liu S. (2022). Separate and integrated thermal management solutions for electric vehicles: A review. *J. Power Sources* **550**:232133. DOI:10.1016/j.jpowsour.2022.232133
13. Zhang Z., Wang J., Feng X., et al. (2018). The solutions to electric vehicle air conditioning systems: A review. *Renew. Sustain. Energy Rev.* **91**:443–463. DOI:10.1016/j.rser.2018.04.005
14. Qin X., Zhang Y., Wang D., et al. (2022). System development and simulation investigation on a novel compression/ejection transcritical CO2 heat pump system for simultaneous cooling and heating. *Energy Convers. Manag.* **259**:115579. DOI:10.1016/j.enconman.2022.115579
15. Ibrahim S. and Mehta R.C. (2018). An investigation of air flow and thermal comfort of modified conventional car cabin using computational fluid dynamics. *J. Appl. Fluid Mech.* **11**:141–150. DOI:10.29252/jafm.11.01.27935
16. Rugh J. and Farrington R. (2007). Vehicle ancillary load reduction project close-out report: An overview of the task and a compilation of the research results. *NREL Tech. Rep.* **540**:42454. DOI:10.2172/922542
17. Shelly T.J., Weibel J.A., Ziviani D., et al. (2021). Comparative analysis of battery electric vehicle thermal management systems under long-range drive cycles. *Appl. Therm. Eng.* **198**:117506. DOI:10.1016/j.applthermaleng.2021.11750
18. Mao Y., Wang J. and Li J. (2018). Experimental and numerical study of air flow and temperature variations in an electric vehicle cabin during cooling and heating. *Appl. Therm. Eng.* **137**:356–367. DOI:10.1016/j.applthermaleng.2018.03.091
19. Zhang H., Dai L., Xu G., et al. (2009). Studies of air-flow and temperature fields inside a passenger compartment for improving thermal comfort and saving energy Part I: Test/numerical model and validation.. *Appl. Therm. Eng.* **29**:2022–2027. DOI:10.1016/j.applthermaleng.2008.10.018
20. Dadour I.R., Almanjahie I., Fowkes N.D., et al. (2011). Temperature variations in a parked vehicle. *Forensic Sci. Int.* **207**:205–211. DOI:10.1016/j.forsciint.2010.10.009
21. Warey A., Kaushik S., Khalighi B., et al. (2020). Data-driven prediction of vehicle cabin thermal comfort: Using machine learning and high-fidelity simulation results. *Int. J. Heat Mass Transf.* **148**:119083. DOI:10.1016/j.ijheatmasstransfer.2019.119083
22. Lee H., Hwang Y., Song I., et al. (2015). Transient thermal model of passenger car's cabin and implementation to saturation cycle with alternative working fluids. *Energy* **90**:1859–1868. DOI:10.1016/j.energy.2015.06.121
23. Horrein L., Bouscayrol A., Lhomme W., et al. (2017). Impact of heating system on the range of an electric vehicle. *IEEE Trans. Veh. Technol.* **66**:4668–4677. DOI:10.1109/TVT.2016.2615095
24. Penning A.K. and Weibel J.A. (2023). Assessing the influence of glass properties on cabin solar heating and range of an electric vehicle using a comprehensive system model. *Appl. Energy* **339**:120973. DOI:10.1016/j.apenergy.2022.120973
25. Xu B. and Arjmandzadeh Z. (2023). Parametric study on thermal management system for the range of full (Tesla Model S)/compact-size (Tesla Model 3) electric vehicles. *Energy Convers. Manag.* **278**:116753. DOI:10.1016/j.enconman.2022.116753
26. Brooker A., Gonder J., Wang L., et al. (2015). FASTSim: A model to estimate vehicle efficiency, cost and performance. *SAE Tech. Pap.* **1**:0973. DOI:10.4271/2015-01-0973
27. Tian Z., Gu B., Gao W., et al. (2020). Performance evaluation of an electric vehicle thermal management system with waste heat recovery. *Appl. Therm. Eng.* **169**:114976. DOI:10.1016/j.applthermaleng.2020.114976
28. Lee S., Chung Y., Kim S., et al. (2023). Predictive optimization method for the waste heat recovery strategy in an electric vehicle heat pump system. *Appl. Energy* **333**:120572. DOI:10.1016/j.apenergy.2022.120572
29. Liu X., Zhang F., Zhang Z., et al. (2024). A three-heat source segmented heating control strategy based on waste heat recovery technology for electric vehicles. *Energy Convers. Manag.* **300**:117932. DOI:10.1016/j.enconman.2024.117932
30. Xue Q., Li J., Ji H., et al. (2024). Sectionalized heating strategy for electric vehicles based on multi-heat-source integrated thermal management system in cold environments. *Appl. Therm. Eng.* **257**:124451. DOI:10.1016/j.applthermaleng.2024.124451
31. Lambora A., Gupta K. and Chopra K. (2019). Genetic algorithm—a literature review. 2019 Int. Conf. Mach. Learn. *Big Data Cloud Parallel Comput.*:380–384. DOI:10.1109/COMITCon.2019.8862255
32. Torregrosa-Jaime B., Bjurling F., Corberán J.M., et al. (2015). Transient thermal model of a vehicle's cabin validated under variable ambient conditions. *Appl. Therm. Eng.* **75**:45–53. DOI:10.1016/j.applthermaleng.2014.12.041
33. Wu J., Jiang F., Song H., et al. (2017). Analysis and validation of transient thermal model for automobile cabin. *Appl. Therm. Eng.* **122**:91–102. DOI:10.1016/j.applthermaleng.2017.04.048
34. Kolhe M., Adhikari S.K. and Muneer T. (2019). Parked electric car's cabin heat management using photovoltaic powered ventilation system. *Appl. Energy* **233**:403–411. DOI:10.1016/j.apenergy.2018.10.012
35. Marcos D., Pino F.J., Bordons C., et al. (2014). The development and validation of a thermal model for the cabin of a vehicle. *Appl. Therm. Eng.* **66**:646–656. DOI:10.1016/j.applthermaleng.2014.02.054
36. Deng L., Li S., Tang X., et al. (2023). Battery thermal- and cabin comfort-aware collaborative energy management for plug-in fuel cell electric vehicles based on the soft actor-critic algorithm. *Energy Convers. Manag.* **283**:116889. DOI:10.1016/j.enconman.2023.116889
37. Chang T., Sheu J., Huang J., et al. (2018). Development of a CFD model for simulating vehicle cabin indoor air quality. *Transp. Res. Part D Transp. Environ.* **62**:433–440. DOI:10.1016/j.trd.2018.03.014
38. Ank M., Sommer A., Abo Gamra K., et al. (2023). Lithium-ion cells in automotive applications: Tesla 4680 cylindrical cell teardown and characterization. *J. Electrochem. Soc.* **170**:120536. DOI:10.1149/1945-7111/ad14d0
39. Wang Z., Ma J. and Zhang L. (2017). Finite element thermal model and simulation for a cylindrical Li-ion battery. *IEEE Access* **5**:15372–15379. DOI:10.1109/ACCESS.2017.2737480
40. Han U., Kang H., Song J., et al. (2021). Development of dynamic battery thermal model integrated with driving cycles for EV applications. *Energy Convers. Manag.* **250**:114882. DOI:10.1016/j.enconman.2021.114882
41. Pozzato G., Allam A., Pulvirenti L., et al. (2023). Analysis and key findings from real-world electric vehicle field data. *Joule* **7**:2035–2053. DOI:10.1016/j.joule.2023.07.009
42. Kuang X., Li K., Xie Y., et al. (2020). Research on control strategy for a battery thermal management system for electric vehicles based on secondary loop cooling. *IEEE Access* **8**:73475–73493. DOI:10.1109/ACCESS.2020.2987885

FUNDING AND ACKNOWLEDGMENTS

This study is supported by the Young Scientists Fund of the National Natural Science Foundation of China (Grant number 52306028), and the HKUST – HKUST (GZ) 20 for 20 Cross-campus Collaborative Research Scheme (Project C006).

AUTHOR CONTRIBUTIONS

Lige Zhao: Conceptualization, Investigation, Methodology, Software, Validation, Visualization, Writing – original draft Parastoo Mohebi: Conceptualization, Investigation, Methodology, Supervision, Writing – review & editing Zhe Wang: Conceptualization, Funding acquisition, Investigation, Methodology, Project administration, Resources, Supervision, Writing – review & editing All authors contributed to the manuscript and approved the final version

DECLARATION OF INTERESTS

The authors declare no competing interests.

DATA AND CODE AVAILABILITY

Data are available from the corresponding author upon reasonable request.

SUPPLEMENTAL INFORMATION

Supplementary materials are available at: https://doi.org/10.59717/ipj.energy-use.2025.100005